VII SEMINAR and WORKSHOP in OCEAN ENGINEERING
Rio Grande, November 23^{rd} to 25^{th}, 2016

ESTIMATE OF THE WAVE CLIMATE ON THE MOST ENERGETIC LOCATIONS OF THE SOUTH-SOUTHEASTERN BRAZILIAN SHELF

Phelype Haron Oleinik[1], **Wilian Correa Marques**[2], **Eduardo de Paula Kirinus**[3]

[1] Federal University of Rio Grande
Graduate Program in Civil, Coastal and Harbour Engineering
Avenida Itália, km 8, CP. 474, Rio Grande, RS, Brazil
e-mail: phe.h.o1@gmail.com
[2] Federal University of Rio Grande
Institute of Mathematics, Statistics and Physics
Avenida Itália, km 8, CP. 474, Rio Grande, RS, Brazil
[3] Federal University of Rio Grande
Institute of Oceanography
Avenida Itália, km 8, CP. 474, Rio Grande, RS, Brazil

ABSTRACT

The wave energy availability has become a field of intensive research around the world. In this sense, this study aims to estimate the wave climate at the most energetic spots on the South-Southeastern Brazilian Shelf (SSBS) as well as the mean annual behavior of the wave power yield at these sites. To achieve this goal, the sea state model TOMAWAC was used to simulate 18 *years of wave conditions on the SSBS which were later converted to a single year, representative of the Brazilian wave climate. The results showed that the sites at Santa Marta cape and Ilhabela are quite similar, with mean wave height of* $1.4\ \mathrm{m}$ *and period of* $8.5\ \mathrm{s}$ *along the climatological year. Farol island, on the other hand, showed higher averages, of* $1.7\ \mathrm{m}$ *and* $8.9\ \mathrm{s}$ *for wave height and period, respectively. The annual behavior of the wave parameters showed greater stability at Santa Marta cape and Ilhabela, and less at Farol island. The wave power yield inherited the characteristics of the other parameters, with an erratic pattern at Farol island and a more behaved one at the other two sites. The mean wave power yield at the Santa Marta cape and Ilhabela is nearly* $10\ \mathrm{kW/m}$ *and at Farol island,* $15\ \mathrm{kW/m}$*. From there on, a wavelet analysis pointed that the most energetic events are those with periods of occurrence from* 6 *to* 12 *days, with the apex at* 7 *days. The wavelet analysis also showed that the most energetic spectrum is the one at Farol island, with* 2.5 *times the energy of the other locations at the period band of* 7 *days.*
Keywords: *Seasonality, TOMAWAC, Wave Climate, Wave Energy*

1. INTRODUCTION

The demand for electricity has increased immensely in the last few decades, and this trend keeps on going. This necessity boosted countless researches in this field. A great deal of these studies focus on clean and renewable energy sources. Ocean wave energy is one of the most environmentally friendly sources of energy since it does not emit pollutants to the atmosphere neither produces harmful waste. Another great positive point about ocean waves is that they are inexhaustible, therefore a power plant could, if correctly operated, provide energy indefinitely.

Though, a few aspects about wave energy must be considered. One of them is the lack of concrete studies on the subject, since it is a rather new technology. What made most of the recent studies on this matter possible is the great advances in computational power, making oceanographic studies in general much easier. With the ease of numerical models and the great development of the third generation models over the last few years, many authors have already published studies on this field.

Wave climatology studies have already been performed by several authors in a global scale. Reguero et al. (2012), for instance, performed a validation and reanalysis of the wave data output by WAVEWATCHIII (WW3) by comparing its results with a combined dataset of different altimeters (Jason 1, Jason 2, TOPEX, ERS-2, Envisat and GFO) and removing outliers due to unusual phenomena that are not predicted by wave models. This work resulted in, what the authors aimed to be, the longest and up-to-date global reanalyzed wave dataset.

Arinaga and Cheung (2012) went further into the wave power issue and used 10 years of hindcast data from WW3 to address the wave power resource and provide an overview of the order of magnitude of wave heights on Earth. Their results presented a cyclic pattern of bigger wave heights hence, wave power, in the winter. This is true to both hemispheres.

Taking the path of seasonal variability, Neill and Hashemi (2013) conducted an analysis of monthly variability of wave power around the British Isles. Their study shown that on the months that comprise the winter (December to March), the wave power availability is remarkably higher than the remaining months. This is mainly due to the passage of severe cold fronts that add up to the waves energy. Neill and Hashemi (2013) also found greater variability associated with the higher wave energies, as well as, interannual variations within the 7 years of data they addressed.

Reguero et al. (2013) used a reanalyzed WW3 dataset on the coastline of South and Central America to characterize the mean behavior and seasonality of waves on these continents. With the 60-year long dataset they also detected a long-term trend of growth of significant wave height along time and created Self Organized Maps for key spots along the South and Central American coastline.

On the Brazilian coast there are a few studies on the subject. Pianca et al. (2010) assessed WW3 reanalyzed data on points scattered along the Brazilian shelf in order to evaluate the representative wave climate of each region throughout the year. Oleinik et al. (2016a) studied the mean behavior of significant wave height (H_s), peak period (T_p), and average direction at the peak period (D_p) on the SSBS as well as the associated energetic potential, in 2006.

Oleinik et al. (2016b) assessed the energetic potential of wind driven waves on the SSBS and concluded that the three locations with the most wave energy availability are, the Santa Marta cape on the state of Santa Catarina, Ilhabela on the state of São Paulo, and Farol island, on the state of Rio de Janeiro. Their results also showed that the most energetic location, Farol island, is also subject to more intense variations along the time.

In order to improve the understanding of the Brazilian wave climate, the aim of this work is to analyze the temporal and spatial variability of the most energetic locations in the studied area constructing wave climate time series for these sites.

To accomplish this goal, the sea state modeling software TOMAWAC was used to simulate 18 years of waves on the South-Southeastern Brazilian Shelf (SSBS), then its results were averaged to a single year, representative of the wave climate on the studied area. The three locations pointed out by Oleinik et al. (2016b) were chosen for the extraction of clustered time series in order to create a wave pattern representative of each site. Finally, the resulting time series were used to create wavelets to represent the variability cycles within a year.

2. MATERIALS AND METHODS

This study addresses the application of the third generation wave model TOMAWAC (TELEMAC-Based Operational Model Addressing Wave Action Computation) to simulate the sea state over the SSBS (Fig. 1a) over a period of 18 years, between 1997 and 2014, and the analysis of time series of significant wave height (H_s), peak period (T_p) and, wave power rate per unit crest length (P_w), extracted from the vicinities of three previously selected sites (Fig. 2).

The spatial domain is represented by an unstructured mesh (Fig. 1b) composed of 205617 nodes with varying relative distance between them (from 8 km near the oceanic boundary to 1 km on the coastline and 100 m on areas of interest). Figure 2 shows the computational domain trimmed at the depth of 200 m for a better coastal representation. TOMAWAC's temporal resolution is one hour for each computation, although, the temporal resolution of the output is rather coarse, 12 hours, due to the final size of the output file.

2.1 Numerical model

The numerical model TOMAWAC was used to perform the simulations. This model is part of the TELEMAC modeling system (`www.opentelemac.org`). TOMAWAC is a third generation wave model that computes the sea state

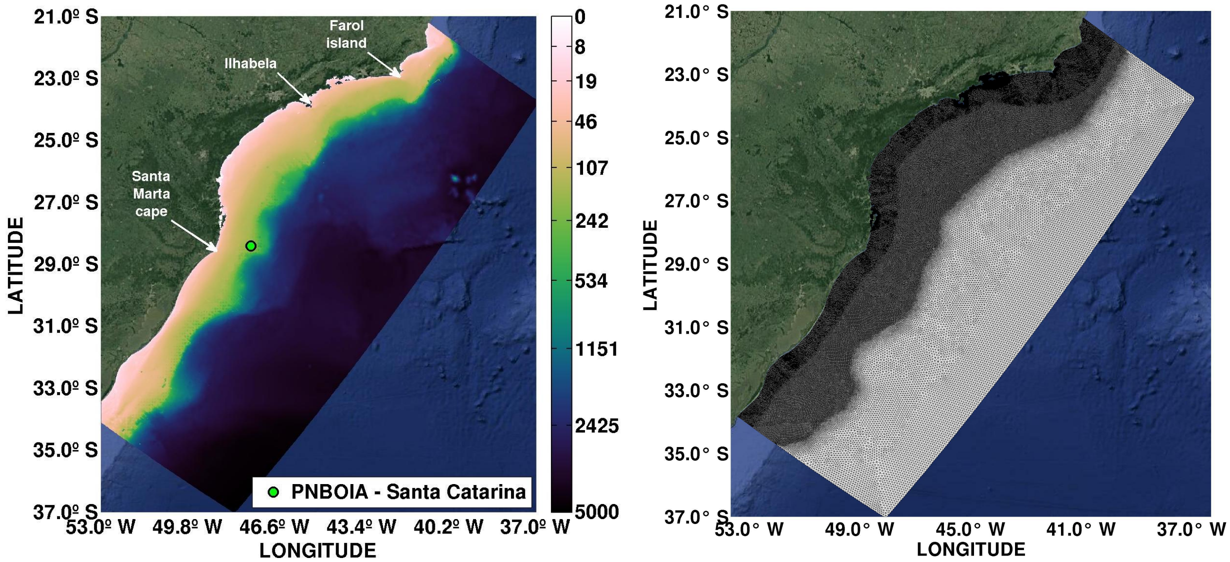

(a) (b)

Figure 1: (a) Bathymetry of the study region. The green dot represents the location of the wave buoy used for the model validation. *Cube Helix* color scheme developed by Green (2011). (b) Unstructured mesh used by TOMAWAC to perform the simulation.

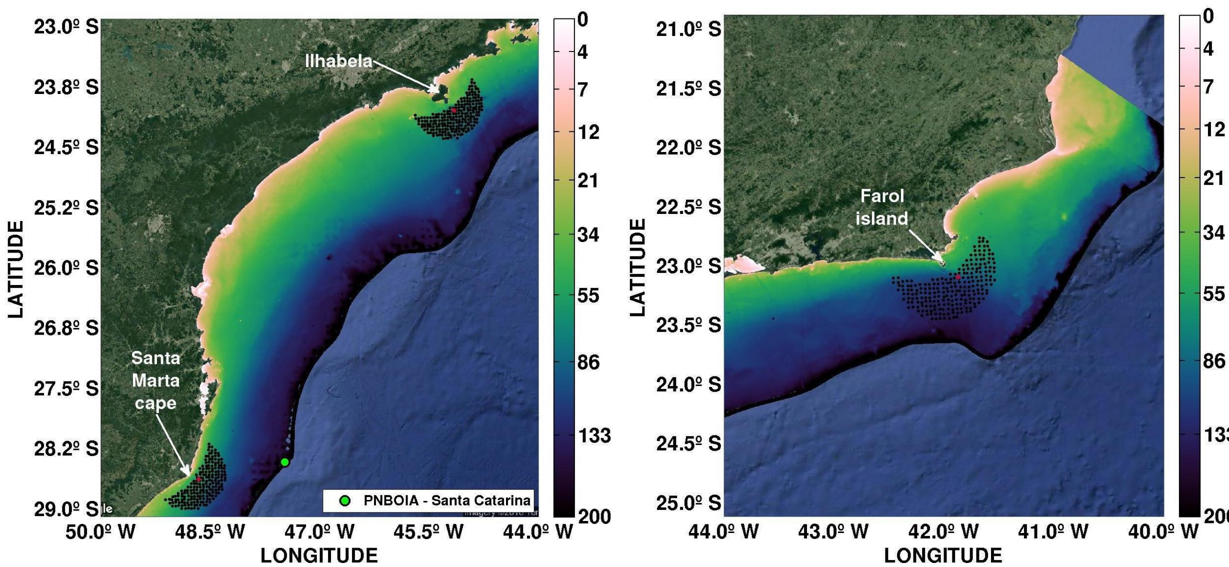

(a) (b)

Figure 2: Bathymetry of the (a) Central part and (b) Northern part of the study region up to 200 m depth. The black dots surrounding the sites indicate the location of the extraction of time series.

by solving the equation of conservation of action density (Eq. (1)) for the wave directional spectrum.

$$\frac{\partial N(f,\theta)}{\partial t} + \frac{\partial \dot{x} N}{\partial x} + \frac{\partial \dot{y} N}{\partial y} + \frac{\partial \dot{k}_x}{\partial k_x} + \frac{\partial \dot{k}_y}{\partial k_y} = Q(k_x, k_y, x, y, t) \tag{1}$$

where N is the directional wave spectrum, x and y are the coordinate system, k_x and k_y are the components on x and y of the wave number vector and t is time. Equation (1) represents that, in a general situation of waves propagating in a non-homogeneous and unsteady environment, the wave action density is preserved within the source and sink terms, defined by Q.

TOMAWAC calculates wind-driven waves taking into account most of the main physical processes involved such as, shoaling, whitecapping, bottom friction-induced dissipation, non-linear interactions between waves and depth-induced refraction. TOMAWAC, however, does not take diffraction and reflection into account.

To solve Eq. (1), TOMAWAC splits the directional spectrum (N) into a finite number of wave frequencies (f_i) and directions (θ_i) and solves Eq. (1) for each component (f_i, θ_i). The directional spectrum of wave energy, denoted by $E(f, \theta)$, can be associated with the directional spectrum of wave action through Eq. (2).

$$E(f,\theta) = N(f,\theta).\rho g \sigma \tag{2}$$

where ρ is the specific mass of water, g is the gravity acceleration and σ is the angular frequency of the waves given by $\sigma = 2\pi f$. The integration of $E(f,\theta)$ along the discretized frequencies and directions yields the energy per unit area of the random multi-directional waves (Equation (3)).

$$\sum_{f}^{f+df} \sum_{\theta}^{\theta+d\theta} \frac{1}{2}\rho g a_m^2 = E(f,\theta) df d\theta \tag{3}$$

2.2 Superficial and Boundary Conditions

To perform the numerical simulations, TOMAWAC was initialized from the rest. The oceanic boundaries were set by the imposition of H_s, T_p and D_p, downloaded from the database generated by the wave forecasting model WAVEWATCHIII (`ftp://polar.ncep.noaa.gov/history/waves`) with spatial and temporal resolution of 30 arc minutes and 3 hours, respectively.

The superficial boundary was forced by winds from NOAA, from the NCEP/NCAR Reanalysis Project (`www.esrl.noaa.gov/psd/data/gridded/data.ncep.reanalysis.html`) with spatial resolution of $1.875°$ and temporal resolution of 6 hours. Both the validation and the climatological simulation used the same data sources. The validation period lasted for 4 years, between 2011 and 2014 and the simulation for the climatological study lasted 18 years from 1997 to 2014 due to availability of data to run TOMAWAC.

2.3 Validation

The results used in this study were previously calibrated by Oleinik et al. (2016b) using buoy data from the *Programa Nacional de Boias* (PNBOIA) for the year of 2012, from buoys located off the coast of the states of Rio Grande do Sul, Santa Catarina and São Paulo.

The use of TOMAWAC on the SSBS was validated through the comparison of time series of the wave parameters output by the model (H_s, T_p and D_p) with the same parameters measured by a wave buoy on the simulated domain.

The data used were measured by *Axys 3 Metre Buoys* operated by the PNBOIA (`www.goosbrasil.org/pnboia`). The buoy is located off the Brazilian coast on the state of Santa Catarina (28°31' 12"S , 47°23' 24"W). Its location is shown in Fig. 1a. The data were measured with the buoy anchored at a depth of 200 m.

The data measured by the buoy was subject to thorough treatment for removal spikes and outliers. Approximately 17% of the original dataset was deleted. The model output was interpolated to fit the buoy data. The comparison of the time series is shown in Fig. 3.

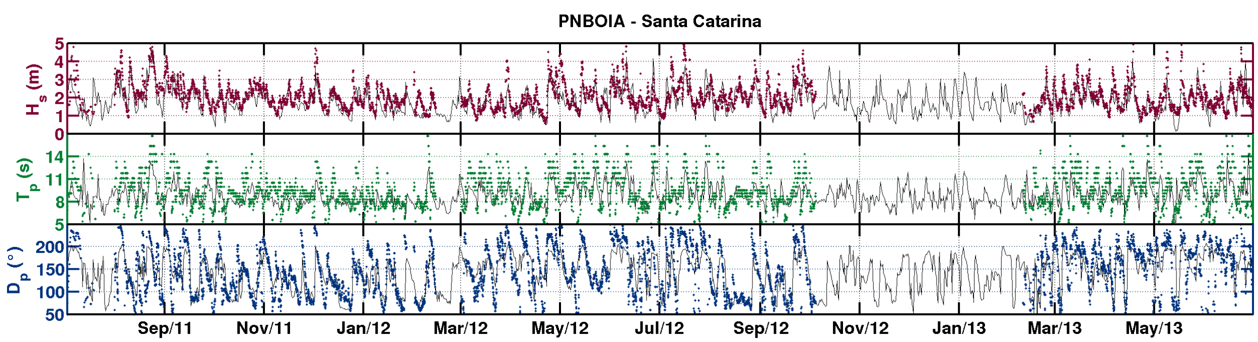

Figure 3: Time series comparing the TOMAWAC output (black line) with the wave parameters, H_s (red dots), T_p (green dots) and D_p (blue dots) measured by the buoy at Santa Catarina.

The time series provide a visual representation of the comparison between TOMAWAC and the buoy. This comparison can be quantified for better understanding, using standard (Janssen et al., 1997; Lalbeharry, 2002; Melo et al., 2008; Chawla et al., 2013) error metrics in this field of study. The equations to compute these metrics are presented in Tab. 1. In the equations, T_i are the data modeled by TOMAWAC, B_i, the data measured by the buoy and n, the number

Table 1: Mathematical equations to compute the error metrics.

Bias	$B = \sum \frac{T_i - B_i}{n}$
Relative Bias	$B_r = {}^{V}/_{\bar{B}}$
Root Mean Square Error	$RMSE = \sqrt{\frac{\sum (T_i - B_i)^2}{n}}$
Symmetric Slope	$SS = \sqrt{\frac{\sum T_i^2}{\sum B_i^2}}$
Correlation Coefficient	$r = \frac{\sum T_i \cdot B_i - n \cdot \bar{T}\bar{B}}{\sqrt{\sum T_i^2 - n \cdot \bar{T}^2} \cdot \sqrt{\sum B_i^2 - n \cdot \bar{B}^2}}$

Table 2: Statistical parameters calculated using the measured data and the TOMAWAC output.

	PARAMETER	PNBOIA SC	TOMAWAC
H_s	Average (m)	1.83	1.77
	Standard Deviation (m)	0.66	0.61
	Mean Relative Error	0.20	
	Root Mean Square Error (m)	0.45	
	Symmetric Slope	0.96	
	Correlation Coefficient	0.76	
T_p	Average (s)	9.64	8.81
	Standard Deviation (s)	2.15	1.20
	Mean Relative Error	0.15	
	Root Mean Square Error (s)	1.78	
	Symmetric Slope	0.90	
	Correlation Coefficient	0.70	
D_p	Average (°)	145.82	141.59
	Standard Deviation (°)	51.41	38.86
	Mean Relative Error	0.20	
	Root Mean Square Error (°)	31.48	
	Symmetric Slope	0.95	
	Correlation Coefficient	0.80	

of data entries in a time series. To complement the results, some statistics about the data from both TOMAWAC and the buoys are presented in Tab. 2 with the error metrics.

The time series (Fig. 3) show a good fit between modeled and measured H_s. The model keeps up to the measured data for both higher and lower waves. For T_p, on the other hand, there is a visible underestimation, by the model, of the actual data. One source of this underestimation can be the frequency distribution of both the model (whose spectrum is discretized along the frequencies) and the buoy (whose output is given in a finite number of frequencies).

For D_p, TOMAWAC results also fit the measured data nicely with, perhaps, a tendency to values slightly lower than the measured. The convention of direction used here is the Nautical Convention (0° points north and directions increase in the clockwise direction) for the direction which the waves are coming from, *e.g.*, 90° waves are waves coming from East and going West.

Firstly, for H_s, the mean values show that, in average, TOMAWAC tends to underestimate the actual wave heights by as little as $6\ \mathrm{cm}$ in both locations. One source of this underestimation may be the temporal resolution of the model output, that can be unaware of high intensity events.

Another reason may be the resolution of the input wind field that, according to a study published by Swail and Cox (2000), the NCEP/NCAR Reanalysis wind fields have a major deficiency for peaks of wave heights that occur during storms, thus justifying the higher wave heights measured by the buoy that are not represented by TOMAWAC. But the model precision cannot be evaluated through mean values only. The standard deviation is approximately the same, but a little higher for the buoy, meaning that its results are more scattered, possibly because of peaks of H_s not represented by TOMAWAC due to the temporal resolution.

An usual error measure is the Mean Relative Error (or Mean Absolute Percentage Error) that, for H_s, is 20%. Though, this error measurement is extremely biased, specially for variables with lower orders of magnitude, so for this type of analysis, it is recommended the use of the Root Mean Square Error ($RMSE$), for it does not have problems with average values close to zero and, mainly, since the difference between model and buoy is squared, bigger differences have more impact on the final value of $RMSE$.

This is useful because numerical models will have acceptable discrepancies compared to the measured data due to minor processes not taken into account, that do not characterize an error. The $RMSE$ for H_s is $0.45\ \mathrm{m}$, acceptable when compared to the studies aforementioned (Janssen et al., 1997; Lalbeharry, 2002; Edwards et al., 2014; Melo et al., 2008).

The Symmetric Slope (SS) acts as the $RMSE$, making bigger values more important, and computing the proportion between modeled and measured values, yielding an average ratio between them. Thus, the SS tells how different are the measurements compared to each other. The SS for H_s is 0.96, meaning that TOMAWAC, in average, tends to give wave heights 96% of the ones measured by the buoy, consolidating the behavior seen in the mean values.

Finally, the correlation coefficient is calculated to show that there is a solid relationship between modeled and measured data. For H_s, the correlation coefficient is 0.76 showing a good linear relationship between model and buoy.

For T_p, both the average and the SS confirm the underestimation seen in Fig. 3. The average has a difference of 0.80 s and the SS is 0.90. The most visible difference is on the standard deviation, for which the buoy yields 2.15 s, and TOMAWAC, 1.20 s, reflecting the fact that the model results of T_p vary from 5 to 14 s while the buoy reaches up to 17 s.

This error may be associated with the poor temporal resolution of the wind input. Also, the study published by Swail and Cox (2000) pointed the issues with the NCEP/NCAR Reanalysis wind fields, which may explain the unconformity of modeled and measured T_p.

The $RMSE$ for T_p is 1.78 s associated with the SS of 0.90, showing the high underestimation by the model. The correlation coefficient is rather fine, because even though there is a strong underestimation tendency, the relationship between modeled and measured T_p is fairly linear.

The D_p comparison is quite good, considering that it is generally the most complicated to reproduce through a model. The average values have a difference of 4.2°, indicating a mean direction of waves from Southeast by South. The standard deviation, on the other hand, is slightly underestimated by TOMAWAC suggesting that the model directions are more restrict to a certain range, which may be due to the disregard of diffraction and reflection.

The $RMSE$ show an error around 31° for D_p, associated with a SS of 0.94 pointing out TOMAWAC's disposition to generate waves with a southern component. Nevertheless, the correlation coefficient shows that there is a strong relationship between modeled and measured data.

3. RESULTS AND DISCUSSION

To create the climatological year for wind driven waves, each set of 18 time steps was averaged resulting in a one year long simulation. Aiming to study the local wave climate, approximately 200 time series of H_s, T_p and D_p were extracted for each of the three selected sites. The location for extraction of the time series is shown in Fig. 2. The black dots in Fig. 4 represent the extracted time series of H_s (first row) and T_p (second row) for each location (columns). These extracted data were averaged in space to obtain a time series that is representative of each site (green lines in Fig. 4).

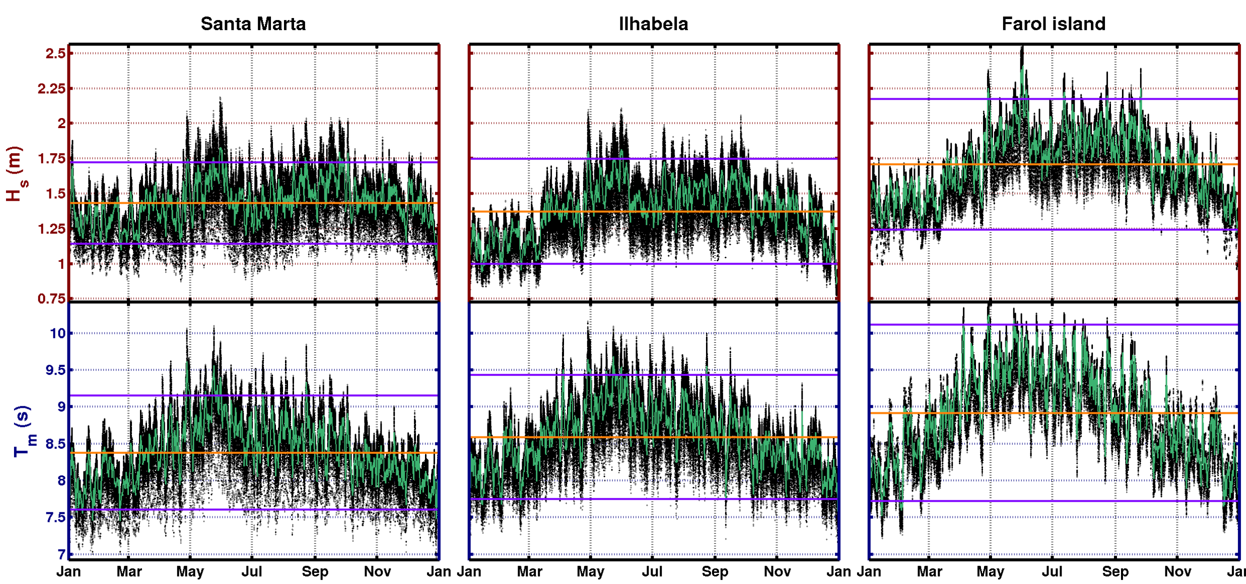

Figure 4: H_s and T_p time series at the three sites. Black dots are the original data and green lines are the spatial average of these data. Orange lines are the temporal average of the data and the purple ones are the average offset by two standard deviations.

Firstly, from Fig. 4, one can see that at Farol island the wave heights are much higher than for Santa Marta cape and Ilhabela. Additionally, the overall aspect of the time series is very similar for Santa Marta cape and Ilhabela, both for H_s and T_p.

The time series of H_s at Santa Marta cape shows little deviation from the mean (orange horizontal line) throughout the year, yet, with a perceivable lower H_s at the ends of the series (corresponding to the summer). The range of H_s, represented by the two standard deviations (purple lines) is also narrow, with a little more than 0.25 m below and above the average. There is also a noticeable rise in H_s in the months of May and September that are approximately the months that mark the transition between cold and warm weather.

The time series of T_p at Santa Marta cape shows a similar behavior but with higher differences between colder and warmer months, presenting higher values in autumn and winter and lower in spring and summer. Also, a significant increase of T_p can be seen in May, aligned to the previously mentioned peak of H_s.

Additionally, at Santa Marta cape, a wide scattering of the black dots can be observed above and below the average. This shows the dissipative characteristic of this location, granting more elevated values to the time series extracted further into the ocean.

As stated before, the behavior observed at Ilhabela is similar to the one at Santa Marta cape, with a slightly lower temporal average and a higher oscillation of the spatial average around it. This can be observed by means of the temporal standard deviation, whose values cover a wider range of H_s. But the overall shape of the series is similar, indicating that most of the atmospheric systems that affect one, also affect the other, resulting in small differences of H_s and T_p between them.

The series of T_p also show that even though the mean H_s is lower at Ilhabela, the waves that reach this location have, in average, higher periods, thus are longer waves. This is associated with the morphology of Ilhabela that, for being extended further into the sea, is affected by the waves before they lose much of their energy.

A striking difference in the series is observed for Farol island. This location is, as Ilhabela, projected towards the ocean but, on the other hand, it is at the tip of the cape of Arraial do Cabo, contrary to Ilhabela, that is more protected within the Santos Basin. This morphological feature makes Farol island directly exposed to ocean waves and, combined with the highly reflexive characteristic of the bathymetry at this location, results in an annual pattern of elevated H_s associated with an also elevated variability along the year. This higher average and deviation is expressed in terms of the elevated average line and much wider region between the lines of the standard deviation.

Another important characteristic of the wave climate at Farol island is the similarity of the raw time series, that do not show much dispersion around the average, compared to Santa Marta cape and Ilhabela. This is, again, an evidence of the low dissipation of the waves as they approach the coastline, characteristic also present in the T_p, that is not significantly changed throughout the site.

One can also observe that, even though the H_s in autumn and winter are higher at Farol island (and as a matter of fact the whole series is), the shape of the line is similar for the three locations, showing a significant growth beyond the average in May, followed by a sudden descent and a more stable form up to September, then dropping below the average again.

This methodology can also be applied to the wave power per unit of crest length (P_w). This result is displayed in Fig. 5 and as one would expect, given the proportionality of a wave energy to its period and the square of its amplitude (Clément et al., 2002), the mean P_w (blue line) on the site of Santa Marta cape is very close to the global average (orange line), deviating a minor amount below it in spring and summer and above, in autumn and winter.

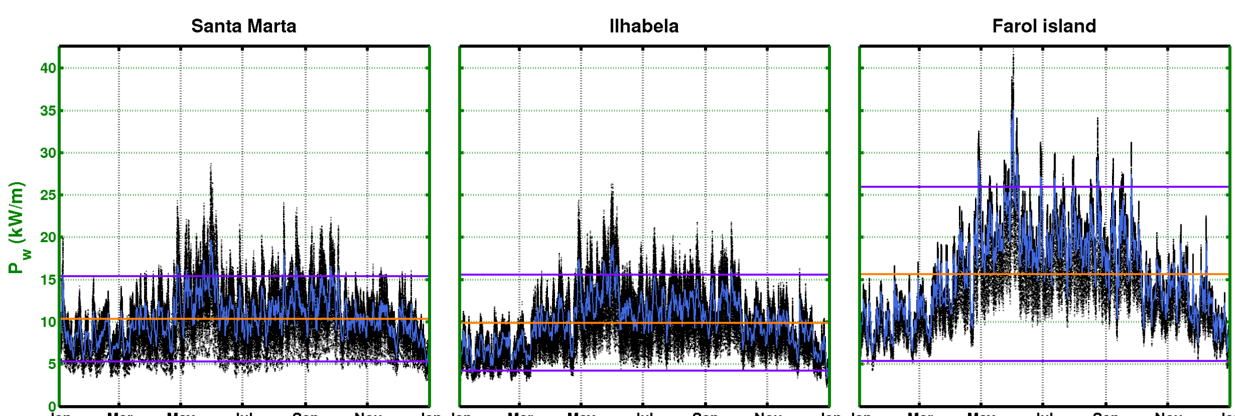

Figure 5: P_w time series at the three sites. Black dots are the original data and blue lines are the spatial average of these data. Orange lines are the temporal average of the data and the purple ones are the average offset by two standard deviations.

The average series of P_w also show a great similarity between Santa Marta cape and Ilhabela, with synchronous occurrences of peaks and depressions. The average values along the time are also quite identical. The main difference between them lies on the dispersion of the raw data, that show a greater scattering at Santa Marta cape due to the higher dissipation of energy at this site.

Recurrently, the series at Farol island show a great difference in comparison with the other two locations, with an average that surpass most of the values found at Santa Marta cape and Ilhabela. It is also clear the huge oscillation around the average presented by this series, notably in autumn and winter.

This series is divided into two clearly different behaviors, of warm and cold seasons. In the warm one, the maximum values hardly surpass the average and do not spread too much around a given values. Otherwise, in colder conditions, the minimum values do not go much below the average, but have a few notable peaks of P_w beyond the upper limit of the two standard deviations. Lastly, one can again see the weak dissipation of the wave energy along the site by the small amount of points scattered below the average series, so few that they do not cause a significant drop blue line.

To conclude the evaluation of the wave climate at these regions, the temporal cycles of variability can be investigated using wavelet analysis following the methodology proposed by Torrence and Compo (1998). The intrinsic biases of the wavelet spectra were removed following the method proposed by Liu et al. (2007).

Figure 6 shows, for the three sites, the same time series of P_w as in Fig. 5, for comparison purposes. The complex valued Paul wavelet spectrum along the climatological year and, the time averaged wavelet power spectrum along the periods are presented.

In the power spectrum of the Fig. 6, lighter regions indicate bigger amounts of energy in the time series, and areas enclosed within the black contours have 95% statistical confidence. The dashed line on the lower part of the spectrum represents the cone of influence, outside of which (hatched zone) border effects are present in the spectrum, thus this area should not be considered. The rightmost figures represent the time averaged power spectrum and the gray dashed line represents the 95% statistical confidence.

The wavelet spectrum at the Santa Marta cape shows the biggest cores of energy within the band of periods from 3 to 10 days, corresponding to the synoptic cycles, associated with the passage of frontal meteorological systems over the region (Marques et al., 2011). The spectrum also shows an elevated peak of energy in the end of April and May and another, steadier, during September, the three of them associated with the peaks of P_w previously mentioned. These peaks are aligned with peaks of fortnightly periods that are not present in the rest of the series.

Additionally, along the autumn and winter parts of the spectrum, there is the transitional presence of energy within the periods between 2 and 4 days and a significant reduction of intensity during warmer months. The time averaged spectrum confirms the strong presence of the energy associated to the synoptic cycles, showing the energy peak on the period of 7 days dropping to half that amount on the time scale of 3 days.

The energy spectrum at Ilhabela shows the same behavior at the period ranges above 7 days, with the high energy event at the end of both April and May. At smaller periods, on the other hand, there is a significant reduction the energy spectra. From November to March there is an almost complete absence of energy in the spectrum, which points to the steadier, warmer climate of this region, contrary to Santa Marta cape that is within a region of interchanged action of warm and cool meteorological systems, which embed a greater deal of energy in the summer part of the spectrum.

Finally, at Farol island, the spectrum is rather similar to the one of Ilhabela, the main reason being the proximity of the sites, both situated at similar latitudes. The main difference between them is a slightly bigger presence of high frequency events in the spectrum of Farol island, possibly due to its greater exposure to meteorological over the waves. The time averaged spectrum at Farol island shows, as expected, a lot more integrated energy (approximately 2.5 times at the period band of 7 days) than the other sites due to the greater amounts of P_w in the time series.

4. CONCLUSION

In order to address the wave conditions on the SSBS, a simulation of 4 years was used with data measured by wave buoys to validate the utilization of the sea state modeling software TOMAWAC on the SSBS, yielding satisfactory comparative statistics for H_s and D_p and a somewhat impaired comparison of T_p. This deficiency is believed to be due to the low temporal and spatial resolution of the wind field used to force the model. Thus, a proposition for future works is the comparison of these results with other simulations using different wind data sets.

The analysis of the spatially averaged time series showed the clear differences in H_s and T_p between summer and winter, the first with lower average and variability and the second, the opposite. The time series also showed that at the Santa Marta cape and at Ilhabela, the wave parameters have smaller averages and are also steadier than at Farol island.

The wavelet analysis showed that the spectrum of the extracted series have a significant amount of energy at the oscillatory scale of 4 to 8 days, as well as a bigger concentration of energy in the time periods correspondent to autumn and winter. It also showed that, as one would expect given the previous results, Farol island has the greatest amount of energy from the three studied sites.

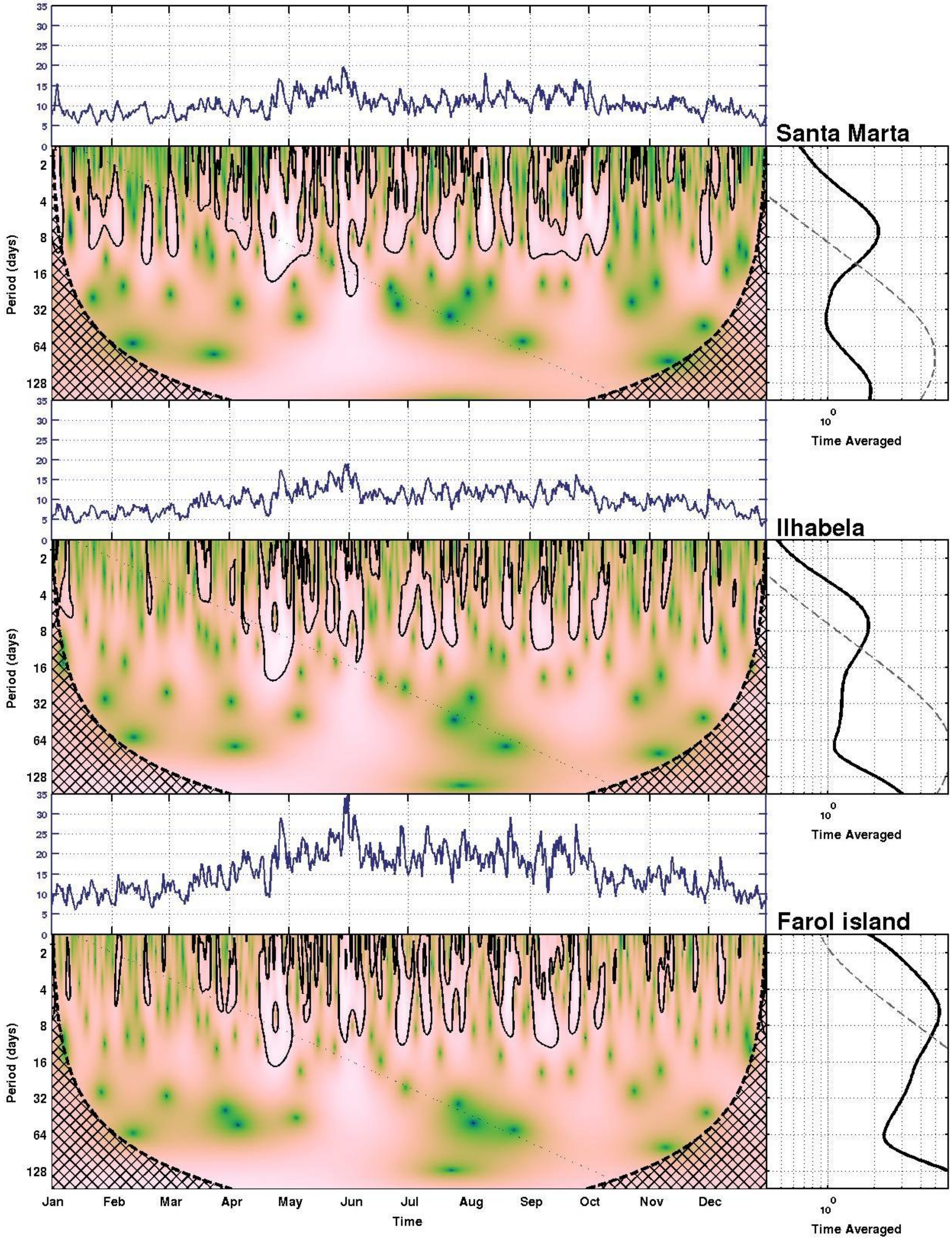

Figure 6: Time series of P_w used for the wavelet analysis, Local Paul wavelet power spectrum and the Time Averaged spectrum at the three studied locations. Thick contour lines on the power spectrum and gray dashed line at the Time Averaged spectrum enclose regions of greater than 95% confidence for a red noise process with a lag 1 coefficient of 0.95.

5. ACKNOWLEDGEMENTS

The authors are grateful to Conselho Nacional de Desenvolvimento Científico e Tecnológico - CNPQ and the "Agência Nacional do Petróleo" - ANP regarding the "Programa de Recursos Humanos" (PRH-27) for the fellowships. The authors are also greatful to the Fundação de Amparo à Pesquisa do Estado do Rio Grande do Sul (FAPERGS) for sponsoring this research under contracts: 1018144 and 1799123, to the Coordenação de Aperfeiçoamento de Pessoal de Nível Superior (CAPES) under contract: 23038.00773/2011-56 and to CNPQ under contract 305885/2013-8.

Additional acknowledgement goes to the Brazilian Navy for providing detailed bathymetric data for the coastal area, NOAA for supplying the wind and wave data sets, and HR Wallingford for providing the academic license for the TELEMAC system to accomplish this research. Research developed with the support of the Centro Nacional de Supercomputação (CESUP) of the Universidade Federal do Rio Grande do Sul (UFRGS).

6. REFERENCES

Arinaga, R.A. and Cheung, K.F., 2012. "Atlas of global wave energy from 10 years of reanalysis and hindcast data". Renewable Energy, Vol 39, No 1, pp. 49–64.

Chawla, A., Spindler, D.M. and Tolman, H.L., 2013. "Validation of a thirty year wave hindcast using the Climate Forecast System Reanalysis winds". Ocean Modelling, Vol 70, pp. 189–206.

Clément, A., McCullen, P., Falcão, A., Fiorentino, A., Gardner, F., Hammarlund, K., Lemonis, G., Lewis, T., Nielsen, K., Petroncini, S., Pontes, M.T., Schild, P., Sjöström, B.O., Sørensen, H.C. and Thorpe, T., 2002. "Wave energy in Europe: Current status and perspectives". Renewable and Sustainable Energy Reviews, Vol 6, No 5, pp. 405–431.

Edwards, E., Cradden, L., Ingram, D. and Kalogeri, C., 2014. "Verification within wave resource assessments. Part 1: Statistical analysis". International Journal of Marine Energy, Vol 8, pp. 50–69.

Green, D.A., 2011. "A colour scheme for the display of astronomical intensity images". Bulletin of the Astronomical Society of India, Vol 39, No 2, pp. 289–295.

Janssen, P.A.E.M., Hansen, B. and Bidlot, J.R., 1997. "Verification of the ECMWF Wave Forecasting System against Buoy and Altimeter Data". American Meteorological Society, Vol 12, pp. 763–784.

Lalbeharry, R., 2002. "Evaluation of the CMC regional wave forecasting system against buoy data". Atmosphere-Ocean, Vol 40, No 1, pp. 1–20.

Liu, Y., Liang, X.S. and Weisberg, R.H., 2007. "Rectification of the Bias in the Wavelet Power Spectrum". Journal of Atmospheric and Oceanic Technology, Vol 24, No 12, pp. 2093–2102.

Marques, W.C., Fernandes, E.H.L. and Rocha, L.A.O., 2011. "Straining and advection contributions to the mixing process in the Patos Lagoon estuary, Brazil". Journal of Geophysical Research, Vol 116.

Melo, E., Hammes, G.R., Franco, D. and Romeu, M.A.R., 2008. "Avaliação de desempenho do modelo WW3 em Santa Catarina". In "Anais do III SEMENGO: Seminario e Workshop em Engenharia Oceanica", Rio Grande, 2008.

Neill, S.P. and Hashemi, M.R., 2013. "Wave power variability over the northwest European shelf seas". Applied Energy, Vol 106, pp. 31–46.

Oleinik, P.H., Marques, W.C. and Kirinus, E.d.P., 2016a. "Simulação de Ondas Oceânicas na Costa Sul-Sudeste Brasileira para Análise do Potencial Energético". Vetor. In Press.

Oleinik, P.H., Marques, W.C., Kirinus, E.P. and Hodapp, M.J., 2016b. "Energetic potential assessment of wind-driven waves on the South-Southeastern Brazilian shelf". Renewable Energy. Article under review.

Pianca, C., Mazzini, P.L.F. and Siegle, E., 2010. "Brazilian offshore wave climate based on NWW3 reanalysis". Brazilian Journal of Oceanography, Vol 58, No 1.

Reguero, B.G., Méndez, F.J. and Losada, I.J., 2013. "Variability of multivariate wave climate in Latin America and the Caribbean". Global and Planetary Change, Vol 100, pp. 70–84.

Reguero, B.G., Menéndez, M., Méndez, F.J., Mínguez, R. and Losada, I.J., 2012. "A Global Ocean Wave (GOW) calibrated reanalysis from 1948 onwards". Coastal Engineering, Vol 65, pp. 38–55.

Swail, V.R. and Cox, A.T., 2000. "On the Use of NCEP-NCAR Reanalysis Surface Marine Wind Fields for a Long-Term North Atlantic Wave Hindcast". Journal of Atmospheric and Oceanic Technology, Vol 17, No 4, pp. 532–545.

Torrence, C. and Compo, G.P., 1998. "A Practical Guide to Wavelet Analysis". Bulletin of the American Meteorological Society, Vol 79, No 1, pp. 61–78.

7. RESPONSIBILITY NOTICE